Influence of the crystalline electrical field on the magnetocaloric effect in the series RNi_2 (R=Pr, Nd, Gd, Tb, Ho, Er)

P. J. von Ranke* and E. P. Nóbrega
Universidade do Estado do Rio de Janeiro, IF, DEQ, Rua São Francisco Xavier 524, 20550-013 Rio de Janeiro, RJ, Brazil

I. G. de Oliveira
Universidade Iguaçu, Avenida Abilio Augusto Távora 2134, 26260, Rio de Janeiro, RJ, Brazil
and Universidade do Grande Rio, Rua Prof. José de Souza Herdy 1160, Duque de Caxias, RJ, Brazil

A. M. Gomes and R. S. Sarthour
Centro Brasileiro de Pesquisas Físicas, Rua Dr. Xavier Sigaud 150, 22290-180, Rio de Janeiro, RJ, Brazil
(Received 19 December 2000; published 16 April 2001)

The magnetocaloric properties in the series RNi_2 (R=Pr, Nd, Gd, Tb, Ho, Er) were fully investigated using a model Hamiltonian that includes the exchange magnetic interaction and the crystalline electrical-field anisotropy. All theoretical results was obtained using the proper model parameters found in the literature for the compounds belonging to this series. For $ErNi_2$ we obtained a good agreement between theoretical and experimental data in the magnetocaloric potentials. An anomalous second peak was predicted to exist in the magnetocaloric curves for $HoNi_2$ and it was ascribed to the high density of states at low temperature.

DOI: 10.1103/PhysRevB.63.184406 PACS number(s): 75.30.Sg, 75.10.Dg, 75.20.En

I. INTRODUCTION

Magnetic refrigeration is based on the magnetocaloric phenomena of the ability of some magnetic materials to heat up when they are magnetized and cool down when removed from the magnetic field. The experimental demonstration of the use of this effect in 1933 to reduce temperature below 1 K lead to a Nobel prize in chemistry for Giauque[1,2] and the following investigations were mainly concerned with obtaining ultralow temperature by extending this technique to nuclear adiabatic demagnetization. More recently, the interest in this research area was considerably increased after Brown[3,4] described a near-room-temperature magnetic refrigerator, using an entropy change process obtained from the paraferromagnetic phase transition in ferromagnetic materials.

In the last decade, much effort has been made to investigate the magnetocaloric potential for different magnetic materials such as amorphous alloys,[5,6] nanocomposites, and superparamagnetic materials.[7–10] An extremely large magnetocaloric effect was recently reported in $La_{0.8}Ca_{0.2}MnO_3$ at $T=230$ K (Ref. 11) and the so-called giant magnetocaloric effect was discovered in $Gd_5Si_2Ge_2$ at $T=276$ K.[12] In both these compounds, the simultaneous structural and magnetic transitions at the Curie temperature are crucial to the large entropy change.

In spite of much magnetocaloric experimental results available nowadays, theoretical investigations are still demanding. Several microscopic theoretical models, already developed to determine the magnetic state of magnetic materials and series of materials, can be applied to best understand and improve the study of the magnetocaloric effect. Recently, theoretical investigations using a Hamiltonian that includes crystalline electrical-field (CEF) interaction predicted an anomalous magnetocaloric effect in paramagnetic $PrNi_5$. This compound cools upon magnetizing and warms upon demagnetizing. This anomaly was experimentally confirmed by heat-capacity measurements.[13] Also, investigations in CEF-magnetic anisotropy in $DyAl_2$ pointed out the existence of an anomaly in its magnetic entropy that consists of an increase in the entropy when the magnetic field is applied in the $\langle 111 \rangle$ direction. This anomaly was associated with the change in the easy direction of magnetization from $\langle 100 \rangle$ to $\langle 111 \rangle$ for a critical applied magnetic field in the $\langle 111 \rangle$ direction.[14]

In this paper we present a full investigation of the magnetocaloric effect in the series RNi_2 (R=Pr, Nd, Gd, Tb, Ho, Er) in which the CEF anisotropy plays a fundamental role, except for Gd, which has no orbital momentum contribution. Besides the CEF, the exchange interaction in molecular-field approximation and the Zeeman effects were included in the model Hamiltonian. From the model Hamiltonian, we determined the two thermodynamic quantities that characterize the magnetocaloric potential: ΔS_{mag} (the isothermal magnetic entropy change) and ΔT_{ad} (the adiabatic temperature change), which are observed upon changes in the external magnetic field[15] as shown in Fig. 1. In the model Hamiltonian, all theoretical results were determined using the proper magnetic parameters for RNi_2 compounds found in the literature. For $HoNi_2$ we theoretically predicted the existence of a second peak in ΔS_{mag} and ΔT_{ad} versus temperature curves in low temperature. This anomalous peak was fully understood and associated with the high density of the CEF state observed in the Lea-Leask-Wolf (LLW) energy-states diagram. An investigation of the CEF quenching effect in the series RNi_2 was also performed using the sum rule from the thermodynamic Maxwell relation. For the $ErNi_2$ compound the comparison between theoretical results and experimental data showed a good agreement, and for others compounds, experimental data was not found.

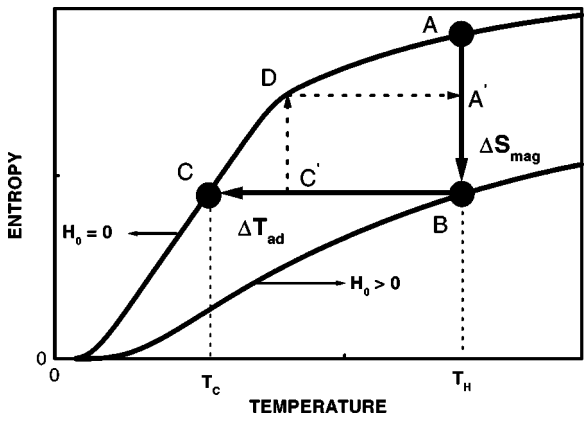

FIG. 1. Typical behaviors for the temperature dependence of the total entropy in a magnetic material, for zero and applied external magnetic field. The arrows $A \rightarrow B$ and $B \rightarrow C$ represent the isothermal entropy and adiabatic temperature changes, respectively. The closed cycle $A' \rightarrow B \rightarrow C' \rightarrow D \rightarrow A'$ is the Carnot cycle.

II. THEORY

The compounds in the series $R\mathrm{Ni}_2$ present cubic symmetry, and therefore, the influence of the electrostatic anisotropy at R ions in $R\mathrm{Ni}_2$ crystals can be described by two parameters in the CEF Hamiltonian. The Ni ion in series $R\mathrm{Ni}_2$ behaves like a nonmagnetic ion, and the magnetic interaction only exists between rare-earth ions. The total Hamiltonian also includes the magnetic term and is given by

$$\hat{H} = \hat{H}_{CEF} + \hat{H}_{MAG}, \tag{1}$$

where

$$\hat{H}_{CEF} = W\left[\frac{X}{F_4}(O_4^0 + 5O_4^4) + \frac{(1-|X|)}{F_6}(O_6^0 + 21O_6^4)\right], \tag{2}$$

and

$$\hat{H}_{MAG} = -g\mu_B H[\cos(\alpha).J^x + \cos(\beta).J^y + \cos(\gamma).J^z]. \tag{3}$$

Equation (2) is the single-ion CEF Hamiltonian written in the LLW notation,[16] where W gives the CEF energy scale and X $(-1<X<1)$ gives the relative contributions of the fourth and sixth degrees in O_n^m, Stevens' equivalent operators.[17] The constants F_4 and F_6 have the values tabulated.[16]

Equation (3) is the single-ion magnetic Hamiltonian, taken in the molecular-field approximation, where g is the Lande factor, μ_B is the Bohr magneton, $H = H_0 + \lambda M$ is the exchange field (external magnetic field plus the effective molecular field) with the molecular-field constant λ, and $M = g\mu_B\langle\cos(\alpha).J^x + \cos(\beta).J^y + \cos(\gamma).J^z\rangle$ being the magnetization in the easy magnetic direction. The symbols $J^\eta, \eta = x,y,z$ stand for the three components of the total angular momentum operator and the cosines are the direction cosines in the crystallographic axis.

The total entropy S_T considered in our lanthanide magnetic systems have mainly three contributions and can be presented as

$$S_T(H_0,T) = S_M(H_0,T) + S_{lat}(T) + S_{el}(T), \tag{4}$$

where S_M is the magnetic entropy, S_{lat} is the entropy of the lattice, and S_{el} is the entropy of the conduction electrons. The magnetic entropy can be determined by the general relation

$$S_M(H_0,T) = \left(\frac{1}{T}\right)\frac{\sum_{k=1}^{2J+1} E_k \exp(-E_k/kT)}{\sum_{k=1}^{2J+1} \exp(-E_k/kT)} + k\ln\left[\sum_{k=1}^{2J+1} \exp(-E_k/kT)\right]. \tag{5}$$

The temperature and field dependence of the above magnetic entropy is not trivial, since for a given pair (H_0,T), the $M = M(H_0,T,M)$ must be determined self-consistently in order to obtain the proper energy eiginvalues E_k from the total Hamiltonian, Eq. (1), to update Eq. (5).

The lattice entropy can be calculated by the Debye interpolation formula

$$S_{lat}(T) = -3R\ln\left[1 - \exp\left(\frac{T}{T_D}\right)\right] + 12R\left(\frac{T}{T_D}\right)^3 \int_0^{T_D/T} \frac{x^3 dx}{\exp(x)-1}, \tag{6}$$

where R is the gas constant and T_D is the Debye temperature. The lattice entropy contribution decreases when T_D increases. The electronic entropy can be obtained from the standard relation

$$S_{el}(T) = \overline{\gamma}T, \tag{7}$$

where $\overline{\gamma}$ is the electronic heat-capacity coefficient.

We are interested in the isothermal magnetic entropy changes $-\Delta S_{mag}$ and the adiabatic temperature change ΔT_{ad} that occur for changes in the external magnetic field. These quantities are obtained from Eqs. (5) and (4), respectively:

$$-\Delta S_M(T,H_0) = S(T,H_0=0) - S(T,H_0), \tag{8}$$

$$\Delta T_{ad} = T_H(T) - T_C(T). \tag{9}$$

The latter quantity is determined by the adiabatic process condition $S_T(H_0,T_H) = S_T(H_0=0,T_C)$ as shown in Fig. 1. In a reversible Carnot cycle, the isothermal heat absorption Q_C and expulsion Q_H, at constant reservoir temperatures T_C and T_H, respectively, are directly related to the refrigerant capacity[15] $Q_H - Q_C = T_H\Delta S_{mag} - T_C\Delta S_{mag} = \Delta T_{ad}\Delta S_{mag}$. It is worth noticing that the higher the two, simultaneously, thermodynamic quantities ΔS_{mag} and ΔT_{ad}, the larger the

TABLE I. Crystalline electrical field, exchange parameters, Curie temperatures, and the easy magnetic directions for the $R\mathrm{Ni}_2$ series.

Compounds	X	W (meV)	λ (T^2/meV)	T_c(K)	Easy direction	References
$GdNi_2$	0	0	93.5 [a]	77.85	[001]	18,19
$PrNi_2$	−0.64	−0.23	115.7	0 [a]	[001] [a]	20
$NdNi_2$	−0.89	0.28	119 [a]	11	[001]	21
$TbNi_2$	−0.73	−0.066	32 [a]	37.5	[111]	21,22
$HoNi_2$	−0.44	0.021	11.3 [a]	15	[001]	21
$ErNi_2$	−0.54	−0.034	10 [a]	7	[001]	23

[a]Parameters determined using the theoretical model.

area in the Carnot cycle ($A' \rightarrow B \rightarrow C' \rightarrow D \rightarrow A'$) will be and therefore the refrigerant capacity of the magnetic material.

In a magnetic system, the variation of the entropy with the external magnetic field depends on the temperature derivative of the magnetization and is given by the Maxwell thermodynamic relation

$$\left(\frac{\partial S}{\partial H_0}\right)_T = \left(\frac{\partial M}{\partial T}\right)_{H_0}. \tag{10}$$

In this way, the isothermal entropy changes, Eq. (8), can be expressed in the general form, i.e., independent of a particular microscopic model as

$$\Delta S(H_0,T) = \int_0^{H_0} \left(\frac{\partial M}{\partial T}\right)_{H_0} dH_0. \tag{11}$$

Integrating over the whole temperature range, an area sum rule can be obtained,

$$-\int_0^{\infty} \Delta S(H_0,T)dT = M_0.\Delta H_0, \tag{12}$$

where M_0 is the magnetization at $T=0$ K. The above relation will be used to study the quenching effect on the magnetic moment in the rare-earth elements in the series $R\mathrm{Ni}_2$.

III. APPLICATION

In Table I is listed the three magnetic parameters, i.e., X, W, and λ, necessary to construct the temperature and field dependence of magnetic entropy for the series $R\mathrm{Ni}_2$, as well as their Curie temperatures and the easy magnetic direction.

In order to best determine the lattice contribution to the total entropy in series $R\mathrm{Ni}_2$, we used the temperature dependence of the Debye temperature for nonmagnetic compounds $LaNi_2$ and $LuNi_2$ obtained from heat-capacity experimental data.[24] The lattice entropy was determined assuming that heat capacity varies linearly in the $R\mathrm{Ni}_2$ series of intermetallic compounds when the R component changes across the series from nonmagnetic La to nonmagnetic Lu. With these assumptions, the expression for the lattice entropy can be determined by the following average expression:

$$S^R_{latt}(T) = \frac{(14-n)S^{La}_{latt}(T) + nS^{Lu}_{latt}(T)}{14}, \tag{13}$$

where n gives the relative position of the rare-earth element in the rare-earth series; in our case we have $n=2,3,7,8,10,11$ for $R=$ Pr, Nd,Gd,Tb,Ho,Er, respectively.

The electronic heat-capacity coefficient $\overline{\gamma}$ for all $R\mathrm{Ni}_2$ compounds considered in this work was $\overline{\gamma} = 5.4\ \mathrm{mJ\,mol^{-1}\,K^{-2}}$, taken from the nonmagnetic compound $LuNi_2$.[25]

IV. RESULTS AND DISCUSSION

Figures 2 and 3 show the temperature dependence of the magnetic entropy changes ΔS_{mag}, and the adiabatic temperature change ΔT_{ad}, respectively, upon changes in the external magnetic field from 0–5 T in the series $R\mathrm{Ni}_2$. Except for $PrNi_2$, which is a paramagnetic compound, all the others compounds are ferromagnetic. The sharp peak in the ΔS_{mag} and ΔT_{ad} curves comes from the paraferromagnetic phase transitions and occurs in the vicinity of the Curie temperatures since, in these regions, the maximum order-disorder magnetic alignment changes take place. Note that there is no ΔS_{mag} and ΔT_{ad} sharp peak in $PrNi_2$, but only a smooth variation due to the Schottky effect in heat capacity, associated with the crystalline electrical-field levels splitting.

For $TbNi_2$, the value $1/\sqrt{3}$ must be considered for the three direction cosines in the magnetic Hamiltonian, Eq. (3)

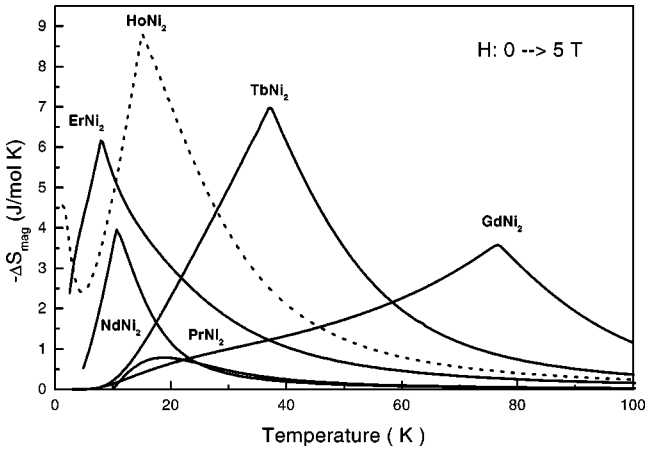

FIG. 2. The temperature dependence of ΔS_{mag} in $R\mathrm{Ni}_2$ for a magnetic-field change from 0–5 T. These curves were obtained using the parameters from Table I. The dotted curve shows the anomalous behavior for the $HoNi_2$ compound.

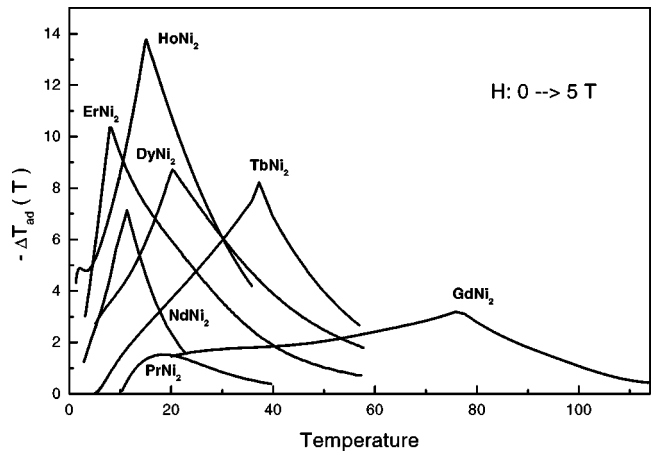

FIG. 3. The temperature dependence of ΔS_{mag} for $R\mathrm{Ni}_2$ for a magnetic-field change from 0–5 T.

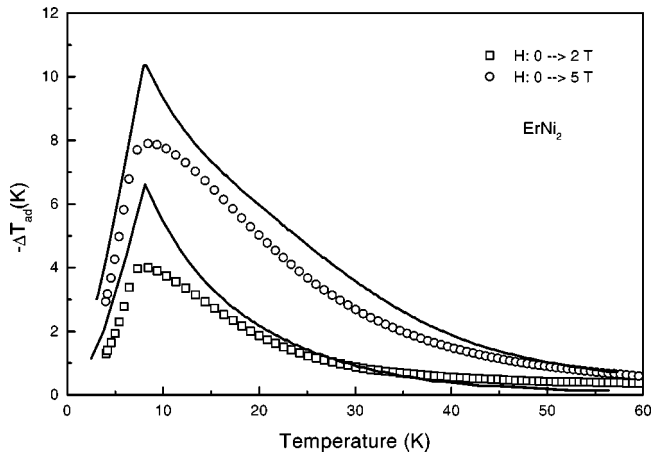

FIG. 5. The temperature dependence of ΔT_{ad} for ErNi_2 for a magnetic-field change from 0–2 and 0–5 T. The solid lines represent the theoretical results and the open circles and squares show experimental data.

to take into account its easy magnetic direction $\langle 111 \rangle$, see Table I. For the other directions, different from the easy magnetic direction, lower values for the magnetocaloric effect were theoretically observed at the Curie temperature.

For ErNi_2 we could compare the theoretical results with the experimental ones for magnetic-field changes from 0–2 and 0–5 T, and a good agreement in both ΔS_{mag} and ΔT_{ad} curves were obtained as shown in Figs. 4 and 5, respectively. The experimental results displayed in Figs. 4 and 5 were obtained by Pecharsky and coworkers[26] at Ames Laboratory using heat-capacity measurements as discussed for similar systems in Ref. 24, DyAl_2, ErAl_2, and DyNi_2. It is worth noticing that the experimental results do not have a sharp peak as displayed in the theoretical curves. The physical origin of this difference is closely related to the short-range order. One would expect that even above the Curie temperature, where the spontaneous magnetization (the long-range order) vanishes, the exchange field will be responsible for some correlations between the directions of neighboring magnetic ions. This effect does not occur when the molecular-field approximation is carried out, as performed in our model.

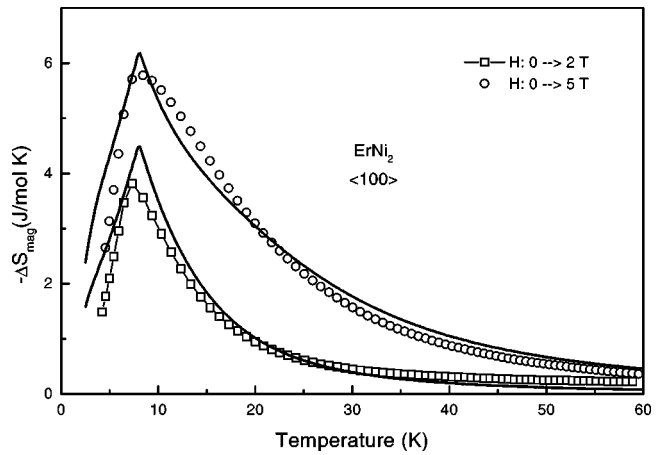

FIG. 4. The temperature dependence of ΔS_{mag} for ErNi_2 for a magnetic-field change from 0–2 and 0–5 T. The solid lines represent the theoretical results and the open circles and squares show experimental data.

We can note that ErNi_2 and NdNi_2 have approximately the same ΔS_{mag} peak temperature but ErNi_2 has a stronger magnetocaloric effect than NdNi_2 (about 56% higher). It means that for the same changes in magnetic field $\Delta H_0 = 5$ T, more heat can be extracted from ErNi_2 ($\Delta Q = T\Delta S$).

From Eq. (5), the maximum magnetic entropy available $S_{mag}^{max} = R \ln(2J+1)$ depends only on the total angular momentum J. Therefore the HoNi_2 compound is expected to produce larger magnetocaloric effects since the Ho ion has the largest total angular momentum in the rare-earth series ($J = 8$). Nevertheless, this argument does not apply in general due to two main reasons: (1) the quenching effects on the orbital contribution to the ionic magnetic moment are due to the CEF interaction and (2) the microscopic mechanisms are responsible for the onset of magnetic order. When the paraferromagnetic transition occurs abruptly, as in the first-order magnetic phase transition, a high magnetocaloric effect is expected. These two points will be discussed below.

A very interesting and anomalous behavior is theoretically predicted to exist in the HoNi_2 compound. Both the ΔS_{mag} and ΔT_{ad} curves present a small second peak at low temperature ($T \sim 1.5$ K). In order to investigate the origin of this anomalous second peak, we plotted the CEF levels scheme as a function of the X-CEF parameter for Ho in the cubic symmetry system, the so-called LLW diagram, see Fig. 6. The vertical dotted line in the LLW diagram, obtained using the proper X-CEF parameter values for HoNi_2 ($X = -0.44$), indicates the ordination of the CEF levels, which are Γ_5^1 (triplet) ground state, Γ^1 (singlet), Γ_4^1 (triplet), Γ_3^1 (doublet), Γ_5^2 (triplet), Γ_4^2 (triplet), and Γ_3^2 (doublet). Consequently, the CEF interaction only partially breaks the $(2J+1)$ Hund's degenerated energy states. These partial energy degenerancies are totally removed by the exchange field. Therefore, considering the exchange field that exists in HoNi_2 at $T = 1.5$ K, which comes from the spontaneous

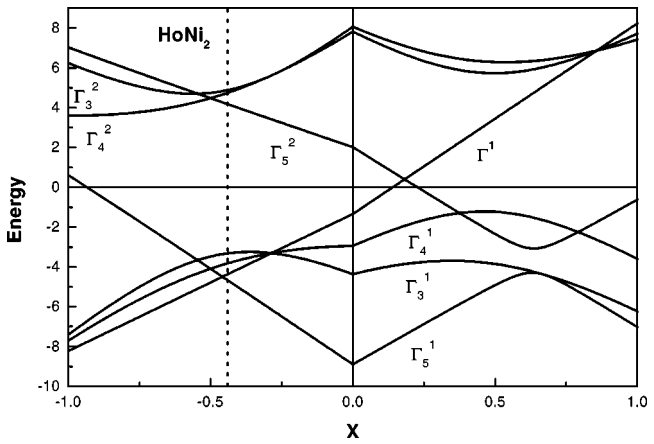

FIG. 6. The LLW diagram for Ho showing the CEF level scheme of $HoNi_2$ along the dotted line at $X=-0.44$.

magnetization ($M/\mu_B=7.96$) at this temperature, we could determine the fully nondegenerated energy diagram shown in the inset of Fig. 7. Figure 7 shows the density of states defined as $2/E_1-E_0$ versus the X-CEF parameter. Here, E_1 and E_0 are the ground and the first excited magnetic energy, respectively. It can be noted that the density of states presents three peaks for the following X-CEF parameters: $X=-0.44$, 0.56, and 1.0. Consequently, the second peak that appears in ΔS_{mag} and ΔT_{ad} curves at about ($T\sim 1.5$ K) in $HoNi_2$ has been understood and connected to the high density of states, since $HoNi_2$ has $X=-0.44$, see Table I. In order to confirm our results, we have performed a theoretical investigation of the other two X parameters, and the second peak at ($T\sim 1.5$ K) was again obtained for $X=0.56$ and 1.0. For other values of the X parameter, only one peak associated with the magnetic phase transition was observed in $HoNi_2$.

A similar anomalous behavior in the magnetocaloric effect in the $(Dy_{1-x}Er_x)$ Al_2 alloy was reported and vastly

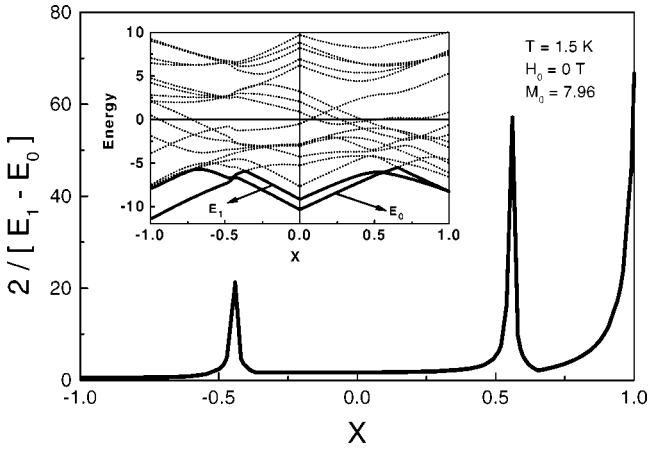

FIG. 7. Density of states for the two lowest levels obtained at $T=1.5$ K versus the X-CEF parameter. For $X=-0.44$ we get the proper $HoNi_2$ curve in Fig. 2 that presents the two peaks. The inset shows the energy-level splittings due to the exchange field at $T=1.5$ K.

TABLE II. From left to the right, for the RNi_2 series the columns give (1) the saturation in gJ per magnetic ion, (2) the area under the ΔS_{mag} versus T curve without CEF interaction, (3) the area under the ΔS_{mag} versus T curve with CEF interaction, and (4) the quenching factor.

Compounds	gJ	Area (tesla) $W=0$	Area (tesla)	QF
$GdNi_2$	7	35	35	1.0
$PrNi_2$	3.2	16	3.71	4.35
$NdNi_2$	3.27	16.35	8.7	1.88
$TbNi_2$	9	45	40.1	1.12
$HoNi_2$	10	50	41	1.21
$ErNi_2$	9	45	24.96, 20.3 [a]	1.82, 2.22 [a]

[a]Indicates the results from experimental data.

studied experimentally by Gschneidner and coworkers using heat-capacity measurements.[27–30]

To investigate the quenching effect in rare-earth ions in the RNi_2 crystal, we used Eq. (12). This relation states that the area under the ΔS_{mag} versus T curves must be equal to the product between the saturation magnetization values per ion M_0 as $T\rightarrow 0$ K and the change in the external magnetic field ΔH_0. In the absence of the CEF and therefore the quenching effect, the saturation magnetization per rare-earth ion is given by the product of the g-factor and the total angular momentum J. In Table II, the second and third columns give the saturation magnetization and the area$=M_0\Delta H_0$ for each magnetic compound, where $\Delta H_0=5$ T and the CEF interaction was neglected ($W=0$). The fourth column gives the area under the ΔS_{mag} versus T curves obtained from Fig. 2, in tesla units. Finally, the last column presents the ratio between these two areas, which we will call from now on, the quenching factor (QF).

$$QF=\frac{area(without-CEF)}{area(with-CEF)}=\frac{[M_0]_{CEF=0}}{[M_0]_{CEF\neq 0}}. \qquad (14)$$

The quenching factor, as defined above, gives the information about the available heat quantity in the whole temperature range that we can extract from the magnetic system when the CEF is present, compared to the free-ions magnetic system. For $GdNi_2$, we have $QF=1$ since Gd presents a $4f$ spin state that does not have CEF perturbation. Therefore, in this point of view, Gd is a good element to be considered as a magnetic materials to be used for refrigerant material. The CEF effect in $PrNi_2$ is very strong and does not allow the existence of a ferromagnetic phase, leading to the highest quenching factor ($QF=4.35$) analyzed in the series RNi_2. Although the Ho presents the highest magnetic moment, the quenching factor in $HoNi_2$ ($QF=1.22$) is higher than $TbNi_2$ ($QF=1.12$). $ErNi_2$ and $NdNi_2$ have approximately the same values for the quenching factor, namely, $QF=1.82$ and 1.88, respectively. Integrating the experimental ΔS_{mag} versus T curve in $ErNi_2$ in Fig. 4, we obtained $QF=2.22$, which is higher than the theoretical prediction. In part, this difference can be attributed to the extrapolation procedure in numerical integration in low-temperature region.

On the other hand, the quenching factor does not give information about how a high magnetocaloric effect can be extracted in an interval temperature range, such as in the vicinity of the Curie temperature. The area sum rule, Eq. (12), states that the area under the ΔS_{mag} versus T curve must be constant. In this way, a high magnetocaloric effect can be obtained in the short temperature region, if outside this region ΔS_{mag} is neglected. Therefore, investigations of microscopic interactions that can be responsible for cumulating area under a small region of ΔS_{mag} versus T (such as interactions that leave the magnetic system to order under first-order transition) can produce, at first, a colossal magnetocaloric effect. The CEF effect produces a reduction in the available area under the ΔS_{mag} versus T curve, as stated by the quenching factor, but, on the other hand, it does not implicate that the CEF anisotropy is opposite to the appearance of the magnetocaloric effect. Actually, the CEF anisotropy, at least theoretically, can bring about a first-order magnetic phase transition,[31,32] and consequently, as discussed above, be responsible for the giant magnetocaloric effect.

It is worth noticing that the quenching factor gives the reduction of the magnetic moment and can be easily determined by heat-capacity measurements with and without magnetic-field application. Also, the magnetocaloric experimental curve ΔS_{mag} versus T provides an excellent way to determine the CEF parameters, since we do not need to take into account the lattice and electronic contribution in the *isotherm* entropy changes, see Eq. (4). We must bear in mind that Eq. (4) was considered for magnetic systems on the assumption that the magnetic-phonon interaction can be neglected.

V. CONCLUSION

We investigated and discussed the main influence of the CEF on the magnetocaloric potential in the $R\mathrm{Ni}_2$ series. A good agreement between the theoretical and experimental data was obtained for ErNi_2, considering that we did not use any fitting procedure. For the other magnetic compounds treated in this work, unfortunately, ΔS_{mag} and ΔT_{ad} data are still lacking. Using the proper CEF and exchange parameters for HoNi_2 we were able to predict an anomalous peak in ΔS_{mag} and ΔT_{ad} curves at about ($T \sim 1.5$ K). This anomalous peak was fully understood and connected to the high density of states that exists in HoNi_2, at low temperature, for the CEF parameter $X = -0.44$. In addition, we performed theoretical analyses of the CEF-quenching effect on the magnetocaloric potential, connected to the sum area rule, that arises in ΔS_{mag} versus temperature behaviors. These studies highlighted the importance of the first-order magnetic phase transition needed to increase the magnetocaloric effect. Earlier investigations[33] of microscopic interaction mechanisms that can improve the magnetocaloric effect and these studies have provided practical interest for producing new refrigerant materials for the magnetic refrigerator.[34]

ACKNOWLEDGMENTS

We thank Professor V. K. Pecharsky for sending us experimental results. We also acknowledge partial support from CNPq, Faperj, and Capes.

*Corresponding author. Email address: vonranke@nitnet.com.br

[1] W.F. Giauque, J. Am. Chem. Soc. **49**, 1870 (1927).
[2] W.F. Giauque and D.P. MacDougall, Phys. Rev. **43**, 768 (1933).
[3] G.V. Brown, J. Appl. Phys. **47**, 3673 (1976).
[4] G.V. Brown, IEEE Trans. Magn. **13**, 1146 (1977).
[5] X.Y. Liu, J.A. Barclay, R.B. Gopal, M. Földeàki, R. Chahine, T.K. Bose, P.J. Schurer, and J.L. LaCombe, J. Appl. Phys. **79**, 1630 (1996).
[6] X.Y. Liu, J.A. Barclay, M. Földeàki, B.R. Gopal, R. Chahine, and T.K. Bose, Adv. Cryog. Eng. **42A**, 431 (1997).
[7] R.D. McMichael, R.D. Shull, L.J. Swartzendruber, and L.H. Bennett, J. Magn. Magn. Mater. **111**, 29 (1992).
[8] L.H. Bennett, R.D. McMichael, L.J. Swartzendruber, R.D. Shull, and R.D. Watson, J. Magn. Magn. Mater. **104**, 1094 (1992).
[9] Robert D. Shull, *Superconductivity and Its Applications*, edited by H. S. Kwok, D. T. Shaw, and M. J. Naughton, AIP Conf. Proc. No. 273 (AIP, New York, 1993), p. 628.
[10] R.D. Shull, R.D. McMichael, and J.J. Ritter, Nanostruct. Mater. **2**, 205 (1993).
[11] Z.B. Guo, Y.W. Du, J.S. Zhu, H. Huang, W.P. Ding, and D. Feng, Phys. Rev. Lett. **78**, 1142 (1997).
[12] V.K. Pecharsky and K.A. Gschneidner, Jr., Phys. Rev. Lett. **78**, 4494 (1997).
[13] P.J. von Ranke, V.K. Pecharsky, K.A. Gschneidner, Jr., and B.J. Korte, Phys. Rev. B **58**, 14 436 (1998).
[14] P.J. von Ranke, I.G. de Oliveira, A.P. Guimarães, and X.A. da Silva, Phys. Rev. B **61**, 447 (2000).
[15] M.E. Wood and W.H. Potter, Cryogenics **25**, 667 (1985).
[16] K.R. Lea, M.J.M. Leask, and W.P. Wolf, J. Phys. Chem. Solids **33**, 1381 (1962).
[17] K.W.H. Stevens, Proc. Phys. Soc., London, Sect. A **65**, 209 (1952).
[18] K. H. J. Bushow, *Ferromagentic Materials*, edited by E. P. Wohlfarth (North-Holland, Amsterdam, 1980), p. 297.
[19] E. Burzo and E.J. Laforest, C R. Acad. Sci. III **27AB**, 114 (1972).
[20] A. Andreeff, Th. Frauenheim, E.A. Goremychkin, H. Griessmann, B. Lippold, W. Matz, O.D. Chistyakov, and E.M. Savitskii, Phys. Status Solidi B **111**, 507 (1982).
[21] E.A. Goremychkin, I. Natkaniec, E. Mühle, and O.D. Chistyakov, J. Magn. Magn. Mater. **81**, 63 (1989).
[22] E. Gratz, E. Goremychkin, M. Latroche, G. Hilscher, M. Rotter, H. Müller, A. Lindbaum, H. Michor, V. Paul-Boncour, and T. Fernandez-Diaz, J. Phys.: Condens. Matter **11**, 7893 (1999).
[23] D. Gignoux and F. Givord, J. Magn. Magn. Mater. **31-34**, 217 (1983).
[24] P.J. von Ranke, V.K. Pecharsky, and K.A. Gschneidner, Jr., Phys. Rev. B **58**, 12 110 (1998).
[25] A.F. Deutz, H.B. Brom, C.D. Wentworth, W.J. Huiskamp, L.J. de Jongh, and K.H.J. Buschow, J. Magn. Magn. Mater. **78**, 176 (1989).
[26] V. K. Pecharsky *et al.* (private communication).
[27] K.A. Gschneidner, Jr., H. Takeya, J.O. Moorman, and V.K. Pe-

charky, Appl. Phys. Lett. **64**, 253 (1994).
[28] K.A. Gschneidner, Jr., H. Takeya, J.O. Moorman, V.K. Pecharsky, S.K. Malik, and C.B. Zimm, Adv. Cryog. Eng. **39**, 1457 (1994).
[29] K.A. Gschneidner, Jr., V.K. Pecharsky, M.J. Gailloux, and H. Takeya, Adv. Cryog. Eng. **42**, 465 (1996).
[30] K.A. Gschneidner, Jr., V.K. Pecharsky, and S.K. Malik, Adv. Cryog. Eng. **42**, 475 (1996).
[31] P.J. von Ranke and N.A. de Oliveira, Physica A **256**, 397 (1998).
[32] N.A. de Lima and V.L. Libero, Phys. Rev. B **61**, 3425 (2000).
[33] I.G. de Oliveira, A. Caldas, E.P. Nobrega, N.A. de Oliveira, and P.J. von Ranke, Solid State Commun. **114**, 487 (2000).
[34] K. A. Gschneidner, Jr. and V. K. Pecharsky, in *Rare Earths: Science, Technology and Application III*, edited by R. C. Bautista, C. O. Bounds, T. W. Ellis, and B. T. Kilbourn (Minerals, Metals & Materials Society, Warendale, PA, 1997).